Single underwater image restoration using attenuation-curve prior

Yi Wang[1], Hui Liu[1] and Lap-Pui Chau[2]
[1]Maritime Institute, [2]School of Electrical and Electronics Engineering,
Nanyang Technological University, Singapore
E-mail: {wang_yi, hui.liu, elpchau}@ntu.edu.sg

***Abstract*—Underwater images suffer from low contrast and color distortion due to the existence of dust-like particles and light attenuation. Some previous works using the patch-based priors, e.g. adaptations of the dark channel prior, cannot achieve satisfactory results in both contrast enhancement and color restoration in the underwater environment. In this paper, we propose a novel underwater image restoration method based on a non-local prior, termed an attenuation-curve prior. This prior relies on the observation that colors of a clear image can be well approximated by several hundred distinct color clusters and the pixels in the same color cluster will form a power function curved line in RGB space after their colors are attenuated by water. Our work mainly contains two steps. Firstly, we estimate the waterlight based on its smoothness properties and the different attenuation coefficient of light. Secondly, we estimate the transmission map using the attenuation-curve prior. Once the waterlight and transmission are obtained, the clear underwater image can be restored. Experimental results demonstrate that our proposed method can achieve better results when comparing with state-of-the-art approaches.**

I. Introduction

Underwater vision plays an important role in ocean engineering and marine scientific research. For example, high-quality underwater images/videos can assist in the subsea exploration and marine geological environment analysis. However, it is not an easy task to improve underwater vision due to light attenuation. The light attenuation is caused by scattering and absorption[1], which significantly degrades the overall performance of underwater imaging systems.

Scattering occurs when light interacts with particles suspended in the imaging medium. It can further be divided into backscattering and forward scattering[2]. Backscattering occurs when the light from ambient illumination sources is scattered into the line of sight (LOS) and eventually reaches the image plane. This results in the haze-like waterlight for underwater images and greatly reduces the scene contrast. Forward scattering takes place when light spreads with small angles relative to LOS. These two effects contribute to the loss of contrast and resolution. Besides, the light absorption rate in water varies between different wavelengths, and so different colors of light will disappear gradually with the increase of the water depth. Since the blue color can penetrate the longest distance in water, the underwater images show a bluish-greenish tone. Therefore, low contrast and color distortion are two major problems we have to deal with.

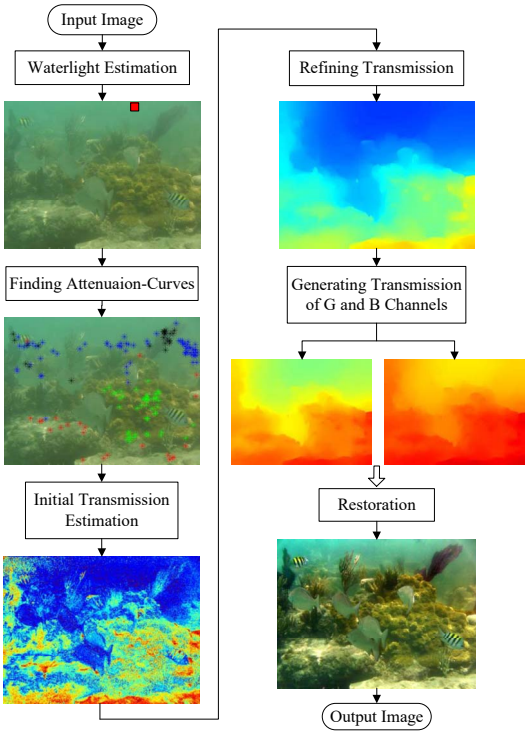

Fig. 1. The flowchart of the proposed method

II. Related Work

Currently, many methods have been proposed to address the above mentioned problems for enhancing the underwater vision. The methods can be classified into two categories. One is the image restoration method which tries to recover the degraded images using the image degradation model. Carlevaris et al. [3] proposed a method to estimate the depth of the scene based on the fact that there is a large difference in attenuation among the three image color channels in the water. Chiang and Chen [1] enhance underwater images by using the dark channel prior algorithm [4] for dehazing and using wavelength compensation for color restoration. Galdran et al. [5] proposed a red channel prior to restore the underwater image. Those techniques are theoretically correct but not feasible in practice because it depends much on estimating some key parameters in the physical model, such as the light scattering and absorption coefficients which may change greatly in different types of water. Another kind is the image enhancement. Ancuti et al. [6] proposed an effective underwater image enhancement method

978-1-4673-6853-7/17/$31.00 ©2017 IEEE

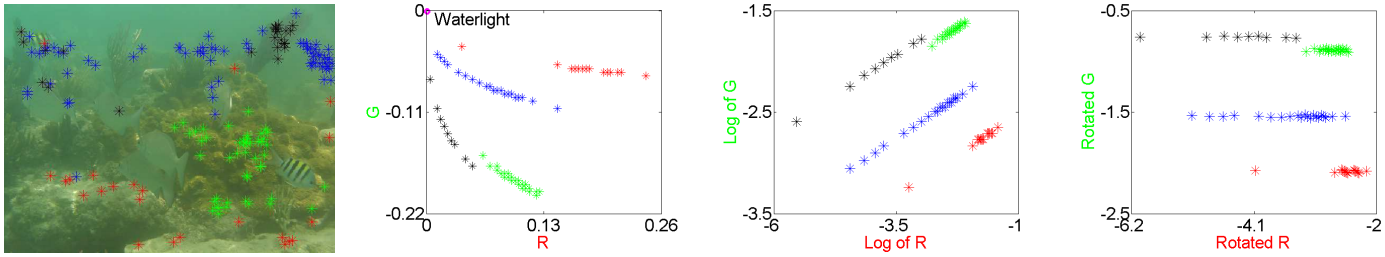

(a) (b) (c) (d)

Fig. 2. The color clusters in the underwater image. (a) Four clusters in the observed image. (b) The power function relationship between the red and green channel. (c) The linear relationship in logarithm. (d) Rotated coordinates for clustering.

by fusion. Methods of this kind only use the qualitative subjective criteria to achieve visually pleasing images. However, the enhancement technique usually produces visually unnatural results because it is not a physics-based approach.

In this paper, we propose a new effective underwater image restoration method based on the attenuation-curve prior. Our method can not only improve the contrast but also remove the color cast. Fig. 1 shows the flowchart of our proposed method. There are two main steps in our method: waterlight estimation and transmission estimation. We will successively describe the detail in the following subsections.

The rest of the paper is organized as follows: Section 3 describes the proposed method in detail. Section 4 presents the experiments result and analysis. Section 5 concludes this paper.

III. The Proposed Method

A. Underwater Image Formation Model

The atmosphere image degradation model in [7], [4] can be extended to the underwater image formation model:

$$I_c(x) = t_c(x) \cdot J_c(x) + (1 - t_c(x)) \cdot B_c,\ c \in \{r, g, b\}, \quad (1)$$

where x represents pixel coordinates, c is the color channel index, I denotes the observed image, J denotes the scene radiance representing the clear image, B denotes the waterlight determined by ambient illumination, and t is the transmission map, which relies on the scene depth $d(x)$ and the wavelength-dependent attenuation coefficient β_c through $e^{-\beta_c d(x)}$. In [5], the transmissions among the RGB channels have a power function relationship:

$$\begin{aligned} t_g(x) &= e^{-\beta_g d(x)} = \left(e^{-\beta_r d(x)}\right)^{\beta_g/\beta_r} = t_r(x)^{\lambda_g}, \\ t_b(x) &= e^{-\beta_b d(x)} = \left(e^{-\beta_r d(x)}\right)^{\beta_b/\beta_r} = t_r(x)^{\lambda_b}, \end{aligned} \quad (2)$$

where λ_g, λ_b are scalar numbers. They are equal to 1 in the atmosphere, but they are less than 1 in the water. Given the observed image, our purpose is to restore the scene radiance by estimating the waterlight and the transmission map.

B. The Prior

We propose a non-local prior, which is inspired by the Haze-Line prior in [8] that describes the difference between the clear image J and the observed image I. In the underwater environment, there are two factors affecting that difference: the varying scene depth $d(x)$ from the camera to objects, which leads to the varying transmission t, and the wavelength-dependent attenuation coefficient β_c, which results in the varying component of the transmission t. We define pixels with the similar color in the clear image as a cluster. Since the pixels of a cluster have disparate scene depths, based on Eq. (1), those pixels will have different captured colors in the observed image after their original colors are attenuated in varying degrees. In RGB space, the former factor arranges those captured pixels in a line, which starts from the original color J (if $t = 1$) and ends at the waterlight color B (if $t = 0$). The latter factor will bend the line to form a power function curved line as showed in Fig. 2(b). Therefore, we term it the attenuation-curve prior.

The attenuation-curve prior can be explained by substituting Eq. (2) into Eq. (1) as follow:

$$(I_c - B_c) = (I_r - B_r)^{\lambda_c} \cdot \left[(J_c - B_c)/(J_r - B_r)^{\lambda_c}\right],\ c \in \{g, b\}. \quad (3)$$

If we define the RGB coordinate space with the waterlight as the origin, the intensity of the green or blue channel $(I_c - B_c)$ of the observed pixels has a power function relationship with that of the red channel $(I_r - B_r)$. Moreover, if the values of B and λ_c are given, the curved line is uniquely determined by the scene radiance J. Different J corresponds to the different curved line. Hence, we can find pixels' original cluster (with the similar scene radiance) of the clear image by clustering them into the curved line in the observed image.

The prior is illustrated in Fig. 2. Fig. 2(a) shows the four clusters with different color markers in the observed image I. Fig. 2(b) shows each curved line consists of different captured pixels, which should belong to the same cluster in clear image J. For better visualization, those lines are projected onto the 2D space (R-G plane). There is a power function relationship between the red and green channel. Based on Eq. (3), this relationship can generalize to 3D space. We will use the prior to estimate transmission in the subsection D.

C. Waterlight Estimation

The waterlight B is the homogeneous background light as a result from backscattering. It is located in the background region and the variance of the pixel values is generally low in this region. To estimate B more reliably, we firstly find the smooth region by empirically dividing the degraded image into 8-by-8 overlapping patches and then choosing the patches with the total variation (TV) less than a predefined threshold.

Within the smooth patches, we calculate the differences between the intensity of the red channel and that of the green and blue channels:

$$D_c(x) = I_c(x) - I_r(x),\ c \in \{g, b\}, \tag{4}$$

where $x \in \mathrm{S}$, $\mathrm{S} = \{\text{all pixels in the chosen patches}\}$. Because the red light attenuates much faster than the green and blue light in the water, those differences for the waterlight are consistently larger. Thus, if R-G channel and R-B channel of a pixel have considerable differences, it seems very likely that the pixel is a candidate for the waterlight.

To find the pixel, we use the index function $\mathrm{Ind}(\cdot)$ to sort the differences D_g and D_b in descending order (e.g., $\mathrm{Ind}_c(1)$ are coordinates of the pixel with the maximum value in D_c):

$$\mathrm{Ind}_c(n) = \mathrm{sort}(D_c(x)),\ c \in \{g, b\}, \tag{5}$$

where $\mathrm{Ind}_c(n)$ outputs indexes (coordinates) of the sort. The intersection $Z = \mathrm{Ind}_g(n \le N) \cap \mathrm{Ind}_b(n \le N)$ can obtain the indexes with the largest values both in D_g and D_b, where N is the number of selected pixels. Thus, the final estimated waterlight B is expressed as:

$$B_c = I_c\left(\arg\max_{x \in Z} I_r(x)\right),\ c \in \{r, g, b\}. \tag{6}$$

Like [4], we consider a pixel with the maximum value of the red channel as the waterlight. The small red rectangle in Fig. 1 indicates the selected waterlight.

D. Transmission Estimation

Transmission estimation is composed of three steps: finding attenuation-curves, estimating an initial transmission, refining the transmission.

Finding Attenuation-Curves: According to the proposed prior, we need to classify pixels into the attenuation-curves in RGB space. But it is difficult to directly classify pixels into curved lines. So we calculate logarithm for Eq. (3):

$$\ln|I_c - B_c| = \lambda_c \ln|I_r - B_r| + \ln\left[|J_c - B_c| / |J_r - B_r|^{\lambda_c}\right], \tag{7}$$

where $c \in \{g, b\}$. Compared to the power function relationship, $\ln|I_c - B_c|$ and $\ln|I_r - B_r|$ follow the linear relationship in RGB space. The lines have the same slope λ_c and a different intercept. The intercept is determined by the scene radiance J. Instead of curved lines, we can classify pixels into the straight lines. The pixels of four straight lines are projected onto the R-G plane as shown in Fig. 2(c).

To speed up the classification process, we rotate the 3D coordinate system to make the R-axis parallel to the direction of the straight lines. In the new coordinate system, it is efficient to cluster the pixels by building a KD-Tree from the predefined tessellation in the G-B plane and querying the tree from G and B coordinates. For better observation, the projected pixels of four lines are rotated in R-G plane as showed in Fig. 2(d). Classifying pixels only need the G coordinates in 2D space. This classification is still valid in 3D space case.

Estimating Initial Transmission: After all pixels are classified into the different attenuation curves, we estimate the transmission for each curved line. We rewrite Eq. (1) as:

$$|I_c(x) - B_c| = t_c(x)\,|J_c(x) - B_c|,\ I_c(x) \in L,\ c \in \{r, g, b\}, \tag{8}$$

Fig. 3. Sample testing images. Left to right, then top to bottom correspond to "image 1" to "image 8", respectively

where L is a curved line. The pixels in L have the same scene radiance J. For a curved line, if $t_c(x) \to 1$, the value of the pixel is nearer to the scene radiance J_c, while if $t_c(x) \to 0$, the value of the pixel is nearer to the waterlight B_c. So, the maximum value of $|I_c - B_c|$ in L is close to $|J_c - B_c|$ and we consider it as the estimation of $|J_c - B_c|$. We obtain a per-pixel estimation of the transmission $\widetilde{t}_c(x)$ for each curved line as follow:

$$\widetilde{t}_c(x) = |I_c(x) - B_c| \,/\, \max_{I_c(x) \in L}\{|I_c(x) - B_c|\}. \tag{9}$$

According to Eq. (2), if λ_g and λ_b are given, we only need to estimate the transmission of one color channel. In the paper, we calculate the transmission of the green channel $\widetilde{t}_r(x)$.

Refining Transmission: Although the above method can obtain the initial transmission, the assumption we use to estimate the value of $|J_c - B_c|$ is not accurate enough if the curved line is very short and near to the waterlight due to the distant scene depth. We use another observation that the transmission map should be patch-wise smooth apart from the depth discontinuities [8]. The transmission is refined by using the same regularization procedure in [8]:

$$\min \sum_x \frac{\left[\hat{t}_r(x) - \tilde{t}_r(x)\right]^2}{\sigma_r(x)} + \lambda \sum_x \sum_{y \in N_x} \frac{\left[\hat{t}_r(x) - \tilde{t}_r(y)\right]^2}{\|I(x) - I(y)\|^2}, \tag{10}$$

where $\hat{t}_r(x)$ is the refined transmission, λ is a regularization parameter to trade off the data and the smoothness terms, N_x is the four nearest neighbors of x, and $\sigma(x)$ is a parameter to measure the reliability of the assumption for $\widetilde{t}_r(x)$. The smaller value of $\sigma(x)$ means $\widetilde{t}_r(x)$ is more reliable. $\sigma(x)$ increases either when there are fewer pixels in the line or when the pixels' values distribution in the line is close to the waterlight.

E. Restoration

Once the waterlight the and refined transmission are estimated, the scene radiance J can be restored by:

$$J_c(x) = \frac{I_c(x) - B_c}{\max(\hat{t}_r(x)^{\lambda_c}, t_0)} + B_c,\ c \in \{r, g, b\}. \tag{11}$$

where $t_0 = 0.1$. Because the recovered image looks dim, we use a global linear contrast stretch (clipping 0.5% the darker and brighter pixels) for display.

IV. EXPERIMENT RESULTS

In this section, for assessing the performance of the proposed method, we compared our method with two state-of-the-art underwater image restoration approaches: Ancuti et al. [6]

(a) (b) (c) (d)

Fig. 4. Results on some of the images. The input images (a) are restored by (b) Ancuti's method[6], (c) Galdran's method [5] and (d) our proposed method.

Fig. 5. Some other results of the proposed method. Row 1 is the input images and row 2 is the corresponding results.

and Galdran et al. [5]. In this paper, we use $\lambda_r = 1$, $\lambda_g = 0.88$ and $\lambda_b = 0.85$ and set $\lambda = 0.1$ in Eq. (10). N equals to 0.1% of the number of chosen pixels, and the number of clusters equals to 400. The 8 images from previous papers [3], [5], [6], [9] are used for the evaluation as showed in Fig. 3.

Three qualitative results of three approaches are demonstrated in Fig. 4. It can be observed that Ancuti's method can significantly increase the contrast and visibility because of their fusion principles, but it may produce an unnatural image (e.g., Image 1) and causes much higher noise (e.g., Image 3). The results of Galdran's method perform well in the more turbid waters, but some restored images have a reddish veil (e.g., Image 1). Our proposed method achieves much better results in the depth-variant scene (e.g., Image 1), and improves the contrast for all images. Some other results of the proposed method are shown in Fig. 5.

In addition to the above subjective measurement, the underwater image quality metrics (UIQM) [10] measurement is utilized to evaluate the performance of the above mentioned methods. The UIQM measurement is composed of underwater image colorfulness measure, underwater image sharpness measure, underwater image contrast measure. The higher the UIQM value, the better the performance is (bold). For the sample testing images, the UIQM values of the restored images by different methods are shown in Table I. It shows our method performs better most of the time.

TABLE I. UIQM VALUES AMONG DIFFERENT METHODS

	Ancuti's method [6]	Galdran's method [5]	Proposed method
Image1	3.6603	5.1546	**5.6469**
Image2	4.1632	3.9564	**4.8030**
Image3	**4.9687**	4.2429	3.6546
Image4	3.7708	4.9065	**5.2659**
Image5	**1.4548**	0.8519	1.1910
Image6	2.8098	**4.3220**	3.4173
Image7	3.2491	4.2363	**4.6655**
Image8	1.2033	2.8511	**3.6573**
Average	3.1600	3.8152	**4.0377**

V. CONCLUSION

In this paper, we proposed a novel attenuation-curve prior for underwater image restoration, which describes that pixels from the same cluster can form a power function curved line in RGB space after attenuation in the water. The proposed method clustered all pixels into attenuation-curves and estimated the transmission from the curved lines. The qualitative results demonstrated our proposed method improves the contrast and removes the color cast. Besides, the quantitative results showed our method outperforms state-of-the-art approaches.

ACKNOWLEDGMENT

The authors would like to thank the Singapore Maritime Institute (SMI) for kindly funding this research project and Fugro Subsea Technologies Pte Ltd providing technical platform for testing and evaluation under the SMI Deepwater Technology $R\&D$ Programme.

REFERENCES

[1] J. Y. Chiang and Y.-C. Chen, "Underwater image enhancement by wavelength compensation and dehazing," *IEEE Trans. Image Process.*, vol. 21, no. 4, pp. 1756–1769, 2012.

[2] Y. Y. Schechner and N. Karpel, "Clear underwater vision," in *Proc. IEEE Conf. Computer Vision and Pattern Recognition*, vol. 1, 2004, pp. I–536.

[3] N. Carlevaris-Bianco, A. Mohan, and R. M. Eustice, "Initial results in underwater single image dehazing," in *Proc. IEEE OCEANS*, 2010, pp. 1–8.

[4] K. He, J. Sun, and X. Tang, "Single image haze removal using dark channel prior," *IEEE Trans. Pattern Anal. Mach. Intell.*, vol. 33, no. 12, pp. 2341–2353, 2011.

[5] A. Galdran, D. Pardo, A. Picón, and A. Alvarez-Gila, "Automatic red-channel underwater image restoration," *Journal of Visual Communication and Image Representation*, vol. 26, pp. 132–145, 2015.

[6] C. Ancuti, C. O. Ancuti, T. Haber, and P. Bekaert, "Enhancing underwater images and videos by fusion," in *Proc. IEEE Conf. Computer Vision and Pattern Recognition*, 2012, pp. 81–88.

[7] W. E. K. Middleton, "Vision through the atmosphere," in *Geophysik II/Geophysics II*. Springer, 1957, pp. 254–287.

[8] D. Berman, S. Avidan *et al.*, "Non-local image dehazing," in *Proc. IEEE Conf. Computer Vision and Pattern Recognition*, 2016, pp. 1674–1682.

[9] J. Xiao, J. Hays, K. A. Ehinger, A. Oliva, and A. Torralba, "Sun database: Large-scale scene recognition from abbey to zoo," in *Proc. IEEE Conf. Computer Vision and Pattern Recognition*, 2010, pp. 3485–3492.

[10] K. Panetta, C. Gao, and S. Agaian, "Human-visual-system-inspired underwater image quality measures," *IEEE J. Ocean. Eng.*, vol. 41, no. 3, pp. 541–551, 2016.